

Quantum Information Scrambling in Quantum Many-body Scarred Systems

Dong Yuan,^{1,*} Shun-Yao Zhang,^{1,*} Yu Wang,² L.-M. Duan,^{1,†} and Dong-Ling Deng^{1,3,‡}

¹Center for Quantum Information, IIIS, Tsinghua University, Beijing 100084, People's Republic of China

²Department of Physics, Harvard University, Cambridge, Massachusetts 02138, USA

³Shanghai Qi Zhi Institute, 41st Floor, AI Tower, No. 701 Yunjin Road, Xuhui District, Shanghai 200232, China

Quantum many-body scarred systems host special non-thermal eigenstates which support periodic revival dynamics and weakly break the ergodicity. In this paper, we study the quantum information scrambling dynamics in quantum many-body scarred systems, with a focus on the “PXP” model. We use the out-of-time-ordered correlator (OTOC) and Holevo information as measures of the information scrambling, and apply an efficient numerical method based on matrix product operators to compute them up to 41 spins. We find that both the OTOC and Holevo information exhibit a linear light cone and periodic oscillations inside the light cone for initial states within the scarred subspace, which is in sharp contrast to thermal or many-body localized systems. To explain the formation of the linear light cone structure, we provide a perturbation-type calculation based on a phenomenological model. In addition, we demonstrate that the OTOC and Holevo information dynamics of the “PXP” model can be measured using the Rydberg-atom quantum simulators with current experimental technologies, and numerically identify the measurable signatures using experimental parameters.

Isolated quantum many-body systems eventually thermalize under the time evolution and their subsystems relax to the equilibrium, leading to the emergence of ergodicity and statistical mechanics. During this process, any local information preserved in the initial states scrambles into the entire system and becomes unrecoverable. This kind of quantum thermalization phenomena has been illustrated by the eigenstate thermalization hypothesis (ETH) in the past decades [1, 2]. While numerous works have confirmed the universality and correctness of ETH in various cases [3–6], discovering quantum many-body systems violating the ETH is still of fundamental and practical importance. Known exceptions to the ETH paradigm include the integrable [7] and many-body localized (MBL) [8] systems, which have either exact or approximate extensive conserved quantities to prevent the systems from thermalization. Recently, in the Rydberg-atom quantum simulation experiments, non-thermal periodic revival dynamics have been observed after quenching the system from a special high-energy Néel state [9, 10]. Following theoretical works attribute this weak ergodicity breaking to a small fraction of ETH-violating eigenstates embedded in a sea of thermal eigenstates, which are named as “quantum many-body scars” [11–13]. In this work, we investigate the information scrambling dynamics in quantum many-body scarred systems (see Fig. 1 for a pictorial illustration).

Quantum information scrambling describes the propagation and effective loss of initial local information in quantum many-body dynamics. The concept of information scrambling exists in multiple contexts, and has attracted considerable attention in many fields, including the black hole thermodynamics [14–16], quantum many-body quench dynamics [17–20] and machine learning [21–23]. For quantum many-body systems with short-range interactions obeying the ETH, the Lieb-Robinson bound [24] restricts the correlation propagation within a linear light cone (analogous to the causal light cone in relativistic theories). In contrast, strong disorders in MBL systems prevent the local transport, resulting in a logarithmic light cone for information spreading [25–30] [see Fig.

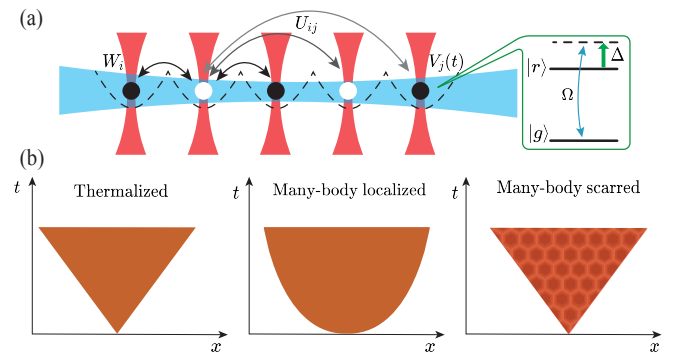


FIG. 1. A schematic illustration of quantum information scrambling dynamics in systems of different thermalization classes and the experimental scheme. (a) The one dimensional Rydberg atom array. Individual neutral atoms are trapped with optical tweezers (vertical red beams). The global Rydberg laser (the horizontal blue beam), with the Rabi frequency Ω and detuning Δ , couples the atomic ground state $|g\rangle$ (black circles) with the Rydberg excited state $|r\rangle$ (white circles). A pair of Rydberg atoms at the distance R_{ij} shares the van der Waals repulsion $U_{ij} = U_0/R_{ij}^6$. The system will be initialized on the $|Z_2\rangle = |grgr \cdots gr\rangle$ state to measure the dynamics of OTOCs $F_{ij}(t) = \langle Z_2 | W_i V_j(t) W_i V_j(t) | Z_2 \rangle$ and Holevo information $\chi_j(t)$. (b) Quantum information scrambling dynamics in thermalized systems (a linear light cone contour), many-body localized systems (a logarithmic light cone contour) and quantum many-body scarred systems (a linear light cone contour and persistent oscillations inside the light cone for initial states within the scarred subspace).

1(b) for a sketch].

Quantum many-body scars, as a new thermalization class in many-body dynamics, possess the potential to exhibit different information spreading behaviours from the former two cases. Despite previous extensive studies of quantum many-body scars from various perspectives [31–57], the explorations of quantum information scrambling in quantum many-body scarred systems are still lacking hitherto. Here, we apply the out-of-time-ordered correlator (OTOC) and Holevo information as measures to study this problem. The exact diagonal-

ization (ED) and an efficient matrix-product-operator (MPO) method [58, 59] are used to conduct extensive numerical calculations. We find that both the OTOC and Holevo information exhibit a linear light cone and periodic revival dynamics inside the light cone for initial states within the scarred subspace, displaying distinct features from the ETH and MBL cases [see a sketch in Fig. 1(b)]. Moreover, the persistent oscillations will disappear and the information propagation speed will increase once we choose generic high-energy initial states. In order to explain the linear light cone structure for the scarred case, we provide a perturbation-type calculation in the interaction picture based on a phenomenological model proposed in [31]. Finally, we propose an experimental measurement protocol for the OTOC and Holevo information dynamics in the Rydberg-atom quantum simulators, and numerically identify the measurable signatures using experimental parameters.

Model.—Motivated by the Rydberg-atom experiment [9], in the limit of Rydberg blockade [60], the physics of quantum many-body scars are extracted as the one-dimensional (1D) “PXP” model [11, 12]:

$$H = \sum_{j=1}^L P_j \sigma_{j+1}^x P_{j+2}, \quad (1)$$

where $P_j = (1 - \sigma_j^z)/2$, $\sigma_j^{x,y,z}$ are Pauli matrices of the j -th qubit, L is the number of total qubits and $|\downarrow\rangle$ ($|\uparrow\rangle$) of the spin-1/2 represent the atomic ground (Rydberg excited) state $|g(r)\rangle$. Below we consider the 1D chain with the open boundary condition. The projectors P_j ensure that adjacent atoms will not be simultaneously excited to the Rydberg states $|r\rangle$ and thus we only consider the dynamics within the constrained Hilbert space (where computational bases with two nearby up spins $|\cdots \uparrow\uparrow \cdots\rangle$ are removed). The PXP Hamiltonian is non-integrable and chaotic according to the level statistics studies, yet it holds a small fraction of ETH-violating scarred eigenstates, which support the periodic revival dynamics of initial states within this scarred subspace (typically the high-energy Néel state $|Z_2\rangle = |\uparrow\downarrow\uparrow\downarrow \cdots \uparrow\downarrow\rangle$), while the Hamiltonian evolution of generic high-energy initial states (like $|0\rangle = |\downarrow\downarrow \cdots \downarrow\rangle$) will quickly become chaotic [11, 12, 32].

The OTOC utilizes the Heisenberg operator growth to characterize the information scrambling and quantum chaos, and is defined as [16, 61, 62]

$$F_{ij}(t) = \langle \psi | W_i^\dagger V_j^\dagger(t) W_i V_j(t) | \psi \rangle, \quad (2)$$

where $|\psi\rangle$ is an initial pure state, W_i, V_j are local observables defined on sites i, j , and $V_j(t) = e^{iHt} V_j e^{-iHt}$ ($\hbar = 1$). The OTOC directly connects to the squared commutator $C_{ij}(t) = \langle \psi | [W_i, V_j(t)]^\dagger [W_i, V_j(t)] | \psi \rangle$ by the relation $C_{ij}(t) = 2(1 - \text{Re}(F_{ij}(t)))$, for unitary operators W_i, V_j . A simple physical picture for the OTOC is that if the Heisenberg operator growth of $V_j(t)$ does not reach the site i , $[W_i, V_j(t)] = 0$, $F_{ij}(t) = 1$, while the equalities will break down when sites i, j become correlated inside the causal region. In the following discus-

sions, we mainly focus on the ZZ -OTOC ($W = \sigma^z, V = \sigma^z$) and XZ -OTOC ($W = \sigma^x, V = \sigma^z$).

The Holevo information (or Holevo χ quantity) originates from the quantum information theory to upper bound the accessible information between two separate agents [63, 64]. Consider that Alice prepares mixed states ρ_X in the set $\{\rho_1, \rho_2, \cdots, \rho_n\}$ with probability $\{p_1, p_2, \cdots, p_n\}$ respectively, and then sends ρ_X to Bob. With any kind of positive operator-valued measures (POVMs), the amount of information Bob can obtain about the variable X according to the measurement outcome Y is bounded by $I(X : Y) \leq \chi = S(\sum_{i=1}^n p_i \rho_i) - \sum_{i=1}^n p_i S(\rho_i)$, where $S(\rho) = -\text{Tr}[\rho \log \rho]$ denotes the von Neumann entanglement entropy. Roughly speaking, the Holevo information describes the distinguishability of states in the set $\{\rho_1, \rho_2, \cdots, \rho_n\}$. For instance, $p_1 = p_2 = 1/2$, if $\rho_1 = |\uparrow\rangle\langle\uparrow|$, $\rho_2 = |\downarrow\rangle\langle\downarrow|$, then $\chi = 1$; while if $\rho_1 = \rho_2 = |\uparrow\rangle\langle\uparrow|$, then $\chi = 0$. Here, we regard the reduced Hamiltonian evolution on subsystems as quantum communication channels in the original setup of Holevo information [63] and use it to study the information scrambling dynamics. Consider the Hamiltonian evolution on two different initial states, $|\psi\rangle$ and $\sigma_i^x |\psi\rangle$, taking $|\psi\rangle$ to be a computational basis (like $|Z_2\rangle$ or $|0\rangle$). Hence, initially we have encoded 1 bit local information at the site i [$|\uparrow(\downarrow)\rangle_i$]. We demonstrate how the 1-bit information scrambles into the entire system by computing the Holevo information on the site j :

$$\chi_j(t) = S\left(\frac{\rho_j(t) + \rho'_j(t)}{2}\right) - \frac{S(\rho_j(t)) + S(\rho'_j(t))}{2}, \quad (3)$$

where $\rho_j(t)$ and $\rho'_j(t)$ are reduced density matrices of the j -th spin after the evolution of the initial state $|\psi\rangle$ and $\sigma_i^x |\psi\rangle$ for some time t . $\chi_j(t)$ measures how much information one could obtain by any local probe on the j -th site for these two sets of evolution.

Numerical simulations.—In Fig. 2 we numerically compute the OTOC and Holevo information for the PXP model as diagnoses of the information scrambling dynamics. Specifically, we apply an efficient MPO method to calculate the ZZ -OTOC and XZ -OTOC up to $L = 41$ spins [65]. We observe the following phenomena: for the initial state $|\psi\rangle = |Z_2\rangle$ [Fig. 2(a), (c)], both the ZZ -OTOC and XZ -OTOC spread ballistically, forming a linear light-cone structure with the butterfly velocity $v_b \sim 0.6$ (inverse of the light cone slope) [15, 59, 66–69]; inside the light cone, the OTOC dynamics show evident periodic revivals with the period $T \approx 4.71$, consistent with the oscillation period of state fidelity and local observables in Hamiltonian evolution [11, 32]. Besides, the oscillations for different sites j are *synchronized*, meaning that $F_{ij}(t)$ of different j have the same period T and reach the maxima at the same time t . In contrast, for a generic high-energy initial state like $|0\rangle$ (Fig. 2(b), (d)), the OTOCs have a larger butterfly velocity $v_b \sim 1$ (information scrambles faster) and decay without discernible periodic revivals inside the light cone.

Since $|Z_2\rangle$ is an eigenstate of the $\sigma_{i(j)}^z$ operator, it seems that the periodic oscillations of the ZZ -OTOC $F_{ij}(t) =$

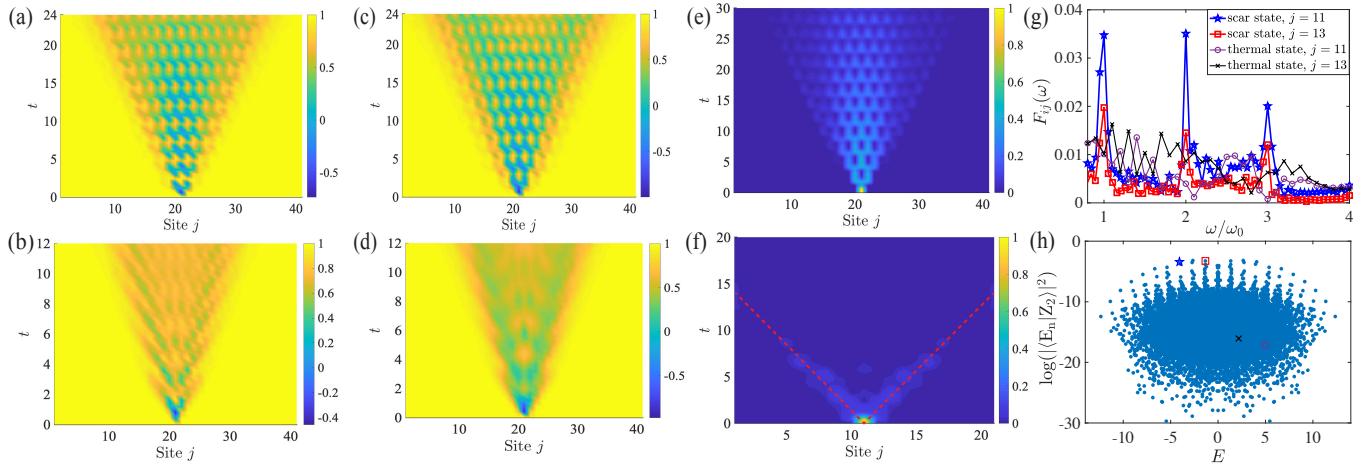


FIG. 2. Quantum information scrambling dynamics in quantum many-body scarred systems. Spatio-temporal evolution of the ZZ -OTOCs (a), (b) and XZ -OTOCs (c), (d) of the PXP model, calculated by the MPO method, with $L = 41$, $i = 21$. The OTOCs $F_{ij}(t)$ exhibit linear light cones and periodic oscillations in (a), (c) with the initial state $|Z_2\rangle$, in contrast to the larger butterfly velocity and absence of oscillations in (b), (d) with the initial state $|0\rangle$. (e), (f) The spatio-temporal evolution of the Holevo information $\chi_j(t)$ for the initial state $|Z_2\rangle$ ($L = 41$, by MPS) and $|0\rangle$ ($L = 21$, by ED). Initially, 1-bit information is encoded in the central qubit. The information travels ballistically and oscillates in (e), while peaks and quickly diminishes in (f) (the peaks of $\chi_j(t)$ for j far from the central qubit are too small to be distinguished, such that are highlighted by red dashed lines). All the color maps are interpolated to non-integer j to better illustrate the light cone. (g) The frequency spectra of the ZZ -OTOC dynamics for the scarred eigenstates (marked by star and square) and thermal eigenstates (marked by circle and cross). (h) The log-scaled overlap between each eigenstate $|E_n\rangle$ and the Z_2 Néel state, $L = 20$, calculated by ED.

$\langle Z_2 | \sigma_i^z \sigma_j^z(t) \sigma_i^z \sigma_j^z(t) | Z_2 \rangle$ can be naively deduced from the approximate recurrence of the $|Z_2\rangle$ state under Hamiltonian evolution [11, 32]. Nevertheless, this simple argument does not apply to the XZ -OTOC case. Furthermore, we numerically show that the persistent and synchronized oscillations still appear even if the initial states are replaced with scarred eigenstates. We use the overlap between eigenstates $|E_n\rangle$ of the PXP Hamiltonian and $|Z_2\rangle$ [Fig. 2(h)], also the half-chain entanglement entropy of $|E_n\rangle$ [65], to distinguish quantum many-body scars from typical thermal eigenstates [11, 12]. In Fig. 2(g), we transform the ZZ -OTOC dynamics into the frequency domain and find that: for initial states being scarred eigenstates, there exist $\omega_0 = 2\pi/T, 2\omega_0, 3\omega_0$ peaks in the spectra for different sites j , but not for the case of initial states being the typical thermal eigenstates. Fig. 2(g) further indicates that the periodic revivals of OTOCs are general phenomena for initial states within the scarred subspace. The recurrence of quantum information signified by the OTOCs is not equivalent to the recurrence of quantum states through Hamiltonian evolution, for which the energy eigenstates actually have *no* dynamics. In [65] we further display the OTOC dynamics with initial states being eigenstates of the PXP Hamiltonian and superposition states of $|Z_2\rangle$ and $|Z'_2\rangle = (\prod_{i=1}^L \sigma_i^x) |Z_2\rangle$.

Similar information scrambling dynamics also emerge when probed by the Holevo information. As shown in Fig. 2(e), for two sets of Hamiltonian evolution on $|Z_2\rangle$ and $\sigma_{[L/2]}^x |Z_2\rangle$, the Holevo information $\chi_j(t)$ initially vanishes everywhere except on the central qubit, where 1 bit local information is encoded. As time evolves, non-zero Holevo in-

formation can be probed at other sites j , which forms a linear light cone in spacetime and also persistent oscillations inside the light cone with a period $T \approx 4.73$, consistent with the OTOC results. In comparison with the initial states $|0\rangle$ and $\sigma_{[L/2]}^x |0\rangle$ [Fig. 2(f)], $\chi_j(t)$ peaks when the information wavefront arrives and eventually diminishes for long time t , following the indistinguishability predicted by the ETH. The information spreading velocity v_h for the $|Z_2\rangle$ case is $v_h \sim 0.6$, less than that of the $|0\rangle$ case $v_h \sim 0.9$. Fig. 2(e) is obtained by the time-evolving block decimation (TEBD) algorithm [70, 71] based on the matrix-product-state (MPS) ansatz, which leverages the relatively low entanglement entropy of scarred eigenstates and is not applicable to the $|0\rangle$ case [11, 12, 65].

Analytical explanations.—The essential features of the PXP model consist of two parts: the periodic oscillations within and the chaotic dynamics out of the scarred subspace, which we adopt a phenomenological model proposed in [31] to effectively describe: $H' = (\Omega/2) \sum_i \sigma_i^x + \sum_i R_{i,i+3} P_{i+1,i+2}$, where $P_{i,i+1} = (1 - \vec{\sigma}_i \cdot \vec{\sigma}_{i+1})/4$, $R_{i,j} = \sum_{\mu,\nu} J_{ij}^{\mu\nu} \sigma_i^\mu \sigma_j^\nu$ ($J_{ij}^{\mu\nu}$ are random coupling constants, $\mu, \nu = \{x, y, z\}$) for a 1D chain with L spins. $H'_0 = (\Omega/2) \sum_i \sigma_i^x$ corresponds to the periodic rotations in the PXP Hamiltonian while $R = \sum_i R_{i,i+3} P_{i+1,i+2}$ plays the role of thermalization for states out of the scarred subspace. The $L + 1$ scarred eigenstates are all the x -direction Dicke states $H'|s = L/2, S^x = m_x\rangle = m_x \Omega |s = L/2, S^x = m_x\rangle$, ($m_x = -s, -s+1, \dots, s-1, s$). Once we start the Hamiltonian evolution from $|\psi\rangle = |\uparrow\uparrow \dots \uparrow\rangle$, perfect quantum state revivals with period $T = 2\pi/\Omega$ will be observed, imitating most but not all the characteristics

of the PXP model [31, 65].

For the non-trivial situation of XZ -OTOC $W_1 = \sigma_1^x$, $V_r = \sigma_r^z$ with the initial state $|\psi\rangle = |\uparrow\uparrow\cdots\uparrow\rangle$, specially at time points $t = nT/2$ ($n = 0, 1, 2, \dots$), the OTOCs are simplified into $F(r, t) = (-1)^n \langle \phi(t) | \sigma_r^z | \phi(t) \rangle$, where $|\phi(t)\rangle = e^{-iH't} \sigma_1^x |\psi\rangle$. The physical picture for the formation of linear light cone structure in OTOC and Holevo information dynamics is that: without the action of σ_1^x , the state $|\phi(t)\rangle$ will undergo perfect periodic oscillations, thus $F(r, t = nT/2) \equiv 1$; However, now σ_1^x penetrates the scarred subspace on the first site. The ‘‘heat flow’’ (like a quasi-particle created by the local quench [20]) leaks and propagates ballistically through the entire system. We use the interaction picture of H'_0 to remove the Rabi oscillation effect. For the early growth region of OTOCs, we can split the evolution time t into r pieces with $\Delta t = t/r$, $J\Delta t \ll 1$, where J is the average energy scale of all the $J_{ij}^{\mu\nu}$. After some lengthy calculations [65], the deterioration of perfect oscillations at the site r will be dominantly caused by an operator product series $\hat{R}^r((r-1)\Delta t) \cdots \hat{R}^2(\Delta t) \hat{R}^1(0)$, [$\hat{R}^i(n\Delta t) = e^{iH'_0 n\Delta t} R_{i,i+3} P_{i+1,i+2} e^{-iH'_0 n\Delta t}$ are operators in the H'_0 interaction picture], which will bound the decay of OTOCs as

$$F(r, t) \sim 1 - \left(\frac{aJt}{r}\right)^r. \quad (4)$$

a is some model-dependent $O(1)$ constant and we have generalized the special time points $t = nT/2$ to arbitrary t before the wavefront arrives [65]. Eq. (4) depicts a linear light cone $t \propto r/J$ in the early growth region of OTOCs. The persistent and synchronized oscillations of the OTOC and Holevo information inside the light cone are attributed to the ‘‘local’’ rather than ‘‘global’’ thermalization and robustness of scarred eigenstates against local perturbations, which are argued in [65] and need future in-depth analytical studies.

Experiment proposals.— Recent experimental progress has enabled the measurements of information scrambling dynamics in well-controlled synthetic quantum systems, including nuclear magnetic resonance (NMR) systems [72, 73], trapped ions [74–77] and superconducting qubits [78–81]. The PXP model can be naturally realized with the Rydberg-atom platform [60, 82, 83], governed by the following Hamiltonian:

$$\mathcal{H} = \frac{\Omega}{2} \sum_i \sigma_i^x - \Delta \sum_i n_i + \sum_{i<j} U_{ij} n_i n_j. \quad (5)$$

σ_i^x connects the atomic ground ($|g\rangle$) and Rydberg excited ($|r\rangle$) state on the site i with the Rabi frequency Ω and detuning Δ . Two Rydberg atoms at distance R_{ij} share the van der Waals repulsion $U_{ij} = U_0/R_{ij}^6$. $n_i = (1 + \sigma_i^z)/2$ denotes the number of Rydberg states. In the parameter regime of Rydberg blockade $U_{i,i+1} = U_1 \gg \Omega \gg U_{i,i+2} = U_2$, $\forall i$, the lowest $U(1)$ symmetry sector $\sum_i n_i n_{i+1} = 0$ of Hamiltonian Eq. (5) approximately reduces to the PXP model, which provides us an opportunity to experimentally measure the ZZ -OTOC and Holevo information dynamics [see Fig. 1(a)].

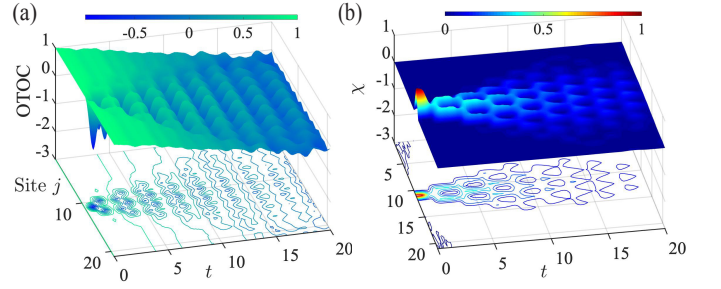


FIG. 3. Numerical simulations of the ZZ -OTOC (a) and Holevo information (b) dynamics for the Rydberg-atom Hamiltonian approximated by \mathcal{H}_\pm , with the initial state $|Z_2\rangle$, under experimental parameters $L = 21$, $\Omega = 2$, $U_1 = 12$, $U_2 = 0.19$ and $\Delta = 0.38$ (by ED). Contour lines of the OTOC and Holevo information χ are projected on the $j - t$ plane.

The main difficulty of simulating OTOC dynamics lies in the implementation of inverse Hamiltonian evolution $\exp(-i(-H)t)$. Fortunately, the PXP model has a particle-hole symmetry operation ($\prod_i \sigma_i^z$) H ($\prod_i \sigma_i^z$) = $-H$ to reverse the sign of H . For the Rydberg-atom Hamiltonian Eq. (5), the $\prod_i \sigma_i^z$ operator only changes the sign of the Rabi oscillation term while keeping the detuning term and Rydberg blockade structure intact. Below we denote the Hamiltonians for experimental evolution and inverse evolution as $\mathcal{H}_\pm = \pm(\Omega/2) \sum_i \sigma_i^x - \Delta \sum_i n_i + U_1 \sum_i n_i n_{i+1} + U_2 \sum_i n_i n_{i+2}$, where we only take the next-nearest-neighbor interaction U_2 into consideration of error analysis due to the sixth power decay. Specifically, for the case of ZZ -OTOC $F_{ij}(t) = \langle \psi | \sigma_i^z \sigma_j^z(t) \sigma_i^z \sigma_j^z(t) | \psi \rangle$ and initial states $|\psi\rangle = |Z_2\rangle$ or $|0\rangle$, since $\sigma_i^z |\psi\rangle = (-1)^{n_i+1} |\psi\rangle$, we have

$$F_{ij}(t) = (-1)^{\langle \psi | n_i | \psi \rangle + 1} \langle \Psi_j(t) | \sigma_i^z | \Psi_j(t) \rangle, \quad (6)$$

where $|\Psi_j(t)\rangle = e^{-i\mathcal{H}_- t} \sigma_j^z e^{-i\mathcal{H}_+ t} |\psi\rangle$, and $e^{-i\mathcal{H}_- t} = (\prod_i \sigma_i^z) e^{-i\mathcal{H}_+ t} (\prod_i \sigma_i^z)$. The measurements of ZZ -OTOC are hence reduced to the evaluation for the expectation value of σ_i^z on a time-dependent quantum state $|\Psi_j(t)\rangle$. The implementation of $|\Psi_j(t)\rangle$ only requires Hamiltonian evolution of Eq. (5) together with global and individual Pauli- Z gates [60, 82]. The measurement protocol for Holevo information follows a straightforward approach as described in the numerical part: preparing two initial states $|Z_2(\mathbf{0})\rangle$ and $\sigma_{\lfloor L/2 \rfloor}^x |Z_2(\mathbf{0})\rangle$, carrying out the Hamiltonian evolution of Eq. (5) independently, doing quantum state tomography for all the single-qubit density matrices, and finally computing $\chi_j(t)$ via Eq. (3).

When approximating the PXP model using the lowest $U(1)$ symmetry sector of the Rydberg-atom Hamiltonian, the errors mainly come from the invalidity of the condition $U_1 \gg \Omega \gg U_2$. Constrained by the geometry of 1D equally-spaced atoms, $U_1/U_2 \sim 64$ is fixed, such that Ω around $\sqrt{U_1 U_2}$ can best fulfill the inequality above. Besides, we numerically observe that a small non-zero Δ in \mathcal{H}_\pm can further eliminate the effect of U_2 , which is probably due to the cancellation of $-\Delta \sum_i n_i$ and $U_2 \sum_i n_i n_{i+2}$ terms on the $|Z_2\rangle$ initial state. The fact

that non-zero detunings amplify the signatures of quantum many-body scars is reminiscent of the recent experiment [10] in which periodically driven detunings stabilize the scar revivals, and might be of independent research interest. In Fig. 3, we display the numerical simulations of the ZZ -OTOC and Holevo information dynamics for the Rydberg-atom Hamiltonian approximated by \mathcal{H}_{\pm} , with the initial state $|Z_2\rangle$, under experimental parameters from [9] and an optimized Δ to increase the oscillation contrast as much as possible [65]. The linear light cone contour and periodic oscillations inside the light cone can be readily observed.

Conclusions and discussions.— In summary, we have numerically calculated the information scrambling dynamics in quantum many-body scarred systems, and found a new paradigm (a linear light cone and periodic oscillations inside the light cone) intrinsically different from the previously studied ETH or MBL cases. Analytical explanations based on perturbation-type calculations are provided [65], yet we expect this work to inspire subsequent in-depth analytical studies, from the perspectives such as Hilbert space fragmentation [46, 47, 84–86], connections to the classical OTOC and chaos theory [32–34, 65, 87, 88], robustness of scarred eigenstates under perturbations [50–54], black hole physics [89, 90], and information scrambling dynamics in other many-body scarred systems [13]. The two criteria, OTOCs and Holevo information, support each other and have been demonstrated to have measurable signatures with current experimental technologies.

We acknowledge helpful discussions with Xun Gao. This work is supported by the Frontier Science Center for Quantum Information of the Ministry of Education of China, Tsinghua University Initiative Scientific Research Program, the Beijing Academy of Quantum Information Sciences, the start-up fund from Tsinghua University (Grant No. 53330300320), the National Natural Science Foundation of China (Grants No. 12075128 and No. 11905108), and the Shanghai Qi Zhi Institute.

* These authors contributed equally to this work.

† lmduan@tsinghua.edu.cn

‡ dldeng@tsinghua.edu.cn

- [1] J. M. Deutsch, “Quantum statistical mechanics in a closed system,” *Phys. Rev. A* **43**, 2046 (1991).
- [2] M. Srednicki, “Chaos and quantum thermalization,” *Phys. Rev. E* **50**, 888 (1994).
- [3] J. M. Deutsch, “Eigenstate thermalization hypothesis,” *Rep. Prog. Phys.* **81**, 082001 (2018).
- [4] H. Kim, T. N. Ikeda, and D. A. Huse, “Testing whether all eigenstates obey the eigenstate thermalization hypothesis,” *Phys. Rev. E* **90**, 052105 (2014).
- [5] J. M. Deutsch, H. Li, and A. Sharma, “Microscopic origin of thermodynamic entropy in isolated systems,” *Phys. Rev. E* **87**, 042135 (2013).
- [6] M. Rigol, V. Dunjko, and M. Olshanii, “Thermalization and its mechanism for generic isolated quantum systems,” *Nature* **452**, 854 (2008).
- [7] B. Sutherland, *Beautiful models: 70 years of exactly solved quantum many-body problems* (World Scientific, 2004).
- [8] D. A. Abanin, E. Altman, I. Bloch, and M. Serbyn, “Colloquium: Many-body localization, thermalization, and entanglement,” *Rev. Mod. Phys.* **91**, 021001 (2019).
- [9] H. Bernien, S. Schwartz, A. Keesling, H. Levine, A. Omran, H. Pichler, S. Choi, A. S. Zibrov, M. Endres, M. Greiner, *et al.*, “Probing many-body dynamics on a 51-atom quantum simulator,” *Nature* **551**, 579 (2017).
- [10] D. Bluvstein, A. Omran, H. Levine, A. Keesling, G. Semeghini, S. Ebadi, T. T. Wang, A. A. Michailidis, N. Maskara, W. W. Ho, *et al.*, “Controlling quantum many-body dynamics in driven rydberg atom arrays,” *Science* **371**, 1355 (2021).
- [11] C. J. Turner, A. A. Michailidis, D. A. Abanin, M. Serbyn, and Z. Papić, “Weak ergodicity breaking from quantum many-body scars,” *Nat. Phys.* **14**, 745 (2018).
- [12] C. J. Turner, A. A. Michailidis, D. A. Abanin, M. Serbyn, and Z. Papić, “Quantum scarred eigenstates in a rydberg atom chain: Entanglement, breakdown of thermalization, and stability to perturbations,” *Phys. Rev. B* **98**, 155134 (2018).
- [13] M. Serbyn, D. A. Abanin, and Z. Papić, “Quantum many-body scars and weak breaking of ergodicity,” *Nat. Phys.* **17**, 675 (2021).
- [14] P. Hayden and J. Preskill, “Black holes as mirrors: quantum information in random subsystems,” *J. High Energy Phys.* **2007**, 120 (2007).
- [15] S. H. Shenker and D. Stanford, “Black holes and the butterfly effect,” *J. High Energy Phys.* **2014**, 1 (2014).
- [16] J. Maldacena, S. H. Shenker, and D. Stanford, “A bound on chaos,” *J. High Energy Phys.* **2016**, 1 (2016).
- [17] R. Lewis-Swan, A. Safavi-Naini, A. Kaufman, and A. Rey, “Dynamics of quantum information,” *Nat. Rev. Phys.* **1**, 627 (2019).
- [18] B. Swingle, “Unscrambling the physics of out-of-time-order correlators,” *Nat. Phys.* **14**, 988 (2018).
- [19] P. Richerme, Z.-X. Gong, A. Lee, C. Senko, J. Smith, M. Foss-Feig, S. Michalakakis, A. V. Gorshkov, and C. Monroe, “Non-local propagation of correlations in quantum systems with long-range interactions,” *Nature* **511**, 198 (2014).
- [20] P. Jurcevic, B. Lanyon, P. Hauke, C. Hempel, P. Zoller, R. Blatt, C. Roos, *et al.*, “Quasiparticle engineering and entanglement propagation in a quantum many-body system,” *Nature* **511**, 202 (2014).
- [21] H. Shen, P. Zhang, Y.-Z. You, and H. Zhai, “Information scrambling in quantum neural networks,” *Phys. Rev. Lett.* **124**, 200504 (2020).
- [22] Y. Wu, P. Zhang, and H. Zhai, “Scrambling ability of quantum neural network architectures,” *Phys. Rev. Research* **3**, L032057 (2021).
- [23] R. J. Garcia, K. Bu, and A. Jaffe, “Quantifying scrambling in quantum neural networks,” [arXiv:2112.01440](https://arxiv.org/abs/2112.01440) (2021).
- [24] E. H. Lieb and D. W. Robinson, “The finite group velocity of quantum spin systems,” *Comm. Math. Phys.* **28**, 251 (1972).
- [25] D.-L. Deng, X. Li, J. H. Pixley, Y.-L. Wu, and S. Das Sarma, “Logarithmic entanglement lightcone in many-body localized systems,” *Phys. Rev. B* **95**, 024202 (2017).
- [26] Y. Huang, Y.-L. Zhang, and X. Chen, “Out-of-time-ordered correlators in many-body localized systems,” *Ann. Phys. (Berlin)* **529**, 1600318 (2017).
- [27] R. Fan, P. Zhang, H. Shen, and H. Zhai, “Out-of-time-order correlation for many-body localization,” *Sci. Bull.* **62**, 707 (2017).
- [28] Y. Chen, “Universal logarithmic scrambling in many body lo-

- calization,” [arXiv:1608.02765](https://arxiv.org/abs/1608.02765) (2016).
- [29] X. Chen, T. Zhou, D. A. Huse, and E. Fradkin, “Out-of-time-order correlations in many-body localized and thermal phases,” *Ann. Phys. (Berlin)* **529**, 1600332 (2017).
- [30] M. C. Bañuls, N. Y. Yao, S. Choi, M. D. Lukin, and J. I. Cirac, “Dynamics of quantum information in many-body localized systems,” *Phys. Rev. B* **96**, 174201 (2017).
- [31] S. Choi, C. J. Turner, H. Pichler, W. W. Ho, A. A. Michailidis, Z. Papić, M. Serbyn, M. D. Lukin, and D. A. Abanin, “Emergent su(2) dynamics and perfect quantum many-body scars,” *Phys. Rev. Lett.* **122**, 220603 (2019).
- [32] W. W. Ho, S. Choi, H. Pichler, and M. D. Lukin, “Periodic orbits, entanglement, and quantum many-body scars in constrained models: Matrix product state approach,” *Phys. Rev. Lett.* **122**, 040603 (2019).
- [33] A. A. Michailidis, C. J. Turner, Z. Papić, D. A. Abanin, and M. Serbyn, “Slow quantum thermalization and many-body revivals from mixed phase space,” *Phys. Rev. X* **10**, 011055 (2020).
- [34] C. J. Turner, J.-Y. Desaulles, K. Bull, and Z. Papić, “Correspondence principle for many-body scars in ultracold rydberg atoms,” *Phys. Rev. X* **11**, 021021 (2021).
- [35] S. Chattopadhyay, H. Pichler, M. D. Lukin, and W. W. Ho, “Quantum many-body scars from virtual entangled pairs,” *Phys. Rev. B* **101**, 174308 (2020).
- [36] N. Maskara, A. A. Michailidis, W. W. Ho, D. Bluvstein, S. Choi, M. D. Lukin, and M. Serbyn, “Discrete time-crystalline order enabled by quantum many-body scars: Entanglement steering via periodic driving,” *Phys. Rev. Lett.* **127**, 090602 (2021).
- [37] B. Mukherjee, S. Nandy, A. Sen, D. Sen, and K. Sengupta, “Collapse and revival of quantum many-body scars via floquet engineering,” *Phys. Rev. B* **101**, 245107 (2020).
- [38] S. Moudgalya, S. Rachel, B. A. Bernevig, and N. Regnault, “Exact excited states of nonintegrable models,” *Phys. Rev. B* **98**, 235155 (2018).
- [39] S. Moudgalya, N. Regnault, and B. A. Bernevig, “Entanglement of exact excited states of affleck-kennedy-lieb-tasaki models: Exact results, many-body scars, and violation of the strong eigenstate thermalization hypothesis,” *Phys. Rev. B* **98**, 235156 (2018).
- [40] M. Schechter and T. Iadecola, “Weak ergodicity breaking and quantum many-body scars in spin-1 xy magnets,” *Phys. Rev. Lett.* **123**, 147201 (2019).
- [41] V. Khemani, C. R. Laumann, and A. Chandran, “Signatures of integrability in the dynamics of rydberg-blockaded chains,” *Phys. Rev. B* **99**, 161101 (2019).
- [42] S. Moudgalya, N. Regnault, and B. A. Bernevig, “ η -pairing in hubbard models: From spectrum generating algebras to quantum many-body scars,” *Phys. Rev. B* **102**, 085140 (2020).
- [43] D. K. Mark and O. I. Motrunich, “ η -pairing states as true scars in an extended hubbard model,” *Phys. Rev. B* **102**, 075132 (2020).
- [44] J.-Y. Desaulles, A. Hudomal, C. J. Turner, and Z. Papić, “Proposal for realizing quantum scars in the tilted 1d fermi-hubbard model,” *Phys. Rev. Lett.* **126**, 210601 (2021).
- [45] S. Scherg, T. Kohler, P. Sala, F. Pollmann, B. H. Madhusudhana, I. Bloch, and M. Aidelsburger, “Observing non-ergodicity due to kinetic constraints in tilted fermi-hubbard chains,” *Nat. Commun.* **12**, 1 (2021).
- [46] C. M. Langlett and S. Xu, “Hilbert space fragmentation and exact scars of generalized fredkin spin chains,” [arXiv:2102.06111](https://arxiv.org/abs/2102.06111) (2021).
- [47] S. Moudgalya, B. A. Bernevig, and N. Regnault, “Quantum many-body scars and hilbert space fragmentation: A review of exact results,” [arXiv:2109.00548](https://arxiv.org/abs/2109.00548) (2021).
- [48] K. Lee, R. Melendrez, A. Pal, and H. J. Changlani, “Exact three-colored quantum scars from geometric frustration,” *Phys. Rev. B* **101**, 241111 (2020).
- [49] J. Jeyaretnam, J. Richter, and A. Pal, “Quantum scars and bulk coherence in a symmetry-protected topological phase,” [arXiv:2103.15880](https://arxiv.org/abs/2103.15880) (2021).
- [50] C.-J. Lin, A. Chandran, and O. I. Motrunich, “Slow thermalization of exact quantum many-body scar states under perturbations,” *Phys. Rev. Research* **2**, 033044 (2020).
- [51] F. M. Surace, M. Votto, E. G. Lazo, A. Silva, M. Dalmonte, and G. Giudici, “Exact many-body scars and their stability in constrained quantum chains,” *Phys. Rev. B* **103**, 104302 (2021).
- [52] I. Mondragon-Shem, M. G. Vavilov, and I. Martin, “Fate of quantum many-body scars in the presence of disorder,” *PRX Quantum* **2**, 030349 (2021).
- [53] K. Huang, Y. Wang, and X. Li, “Stability of 2d quantum many-body scar states against random disorder,” [arXiv:2102.08241](https://arxiv.org/abs/2102.08241) (2021).
- [54] F. M. Surace, M. Dalmonte, and A. Silva, “Quantum local random networks and the statistical robustness of quantum scars,” [arXiv:2107.00884](https://arxiv.org/abs/2107.00884) (2021).
- [55] J. Ren, C. Liang, and C. Fang, “Quasisymmetry groups and many-body scar dynamics,” *Phys. Rev. Lett.* **126**, 120604 (2021).
- [56] C. M. Langlett, Z.-C. Yang, J. Wildeboer, A. V. Gorshkov, T. Iadecola, and S. Xu, “Rainbow scars: From area to volume law,” [arXiv:2107.03416](https://arxiv.org/abs/2107.03416) (2021).
- [57] Z. Yao, L. Pan, S. Liu, and H. Zhai, “Quantum many-body scars and quantum criticality,” [arXiv:2108.05113](https://arxiv.org/abs/2108.05113) (2021).
- [58] S. Xu and B. Swingle, “Accessing scrambling using matrix product operators,” *Nat. Phys.* **16**, 199 (2020).
- [59] S.-Y. Zhang and D.-L. Deng, “Anomalous quantum information scrambling for F_3 parafermion chains,” *Phys. Rev. B* **103**, 195156 (2021).
- [60] M. Saffman, T. G. Walker, and K. Mølmer, “Quantum information with rydberg atoms,” *Rev. Mod. Phys.* **82**, 2313 (2010).
- [61] A. Larkin and Y. N. Ovchinnikov, “Quasiclassical method in the theory of superconductivity,” *Sov Phys JETP* **28**, 1200 (1969).
- [62] K. Hashimoto, K. Murata, and R. Yoshii, “Out-of-time-order correlators in quantum mechanics,” *J. High Energy Phys.* **2017**, 1 (2017).
- [63] A. S. Holevo, “Bounds for the quantity of information transmitted by a quantum communication channel,” *Probl. Inf. Transm.* **9**, 3 (1973).
- [64] M. A. Nielsen and I. L. Chuang, *Quantum Computation and Quantum Information* (Cambridge university press, 2010).
- [65] See Supplemental Materials at [URL will be inserted by publisher] for details on analytical explanations, the MPO and MPS algorithm, and more numerical results, which further includes Refs. [91–101].
- [66] D. A. Roberts and B. Swingle, “Lieb-robinson bound and the butterfly effect in quantum field theories,” *Phys. Rev. Lett.* **117**, 091602 (2016).
- [67] C. Stahl, V. Khemani, and D. A. Huse, “Asymmetric butterfly velocities in hamiltonian and circuit models,” [arXiv:1812.05589](https://arxiv.org/abs/1812.05589) (2018).
- [68] Y.-L. Zhang and V. Khemani, “Asymmetric butterfly velocities in 2-local hamiltonians,” *SciPost Phys.* **9**, 024 (2020).
- [69] F. Liu, J. R. Garrison, D.-L. Deng, Z.-X. Gong, and A. V. Gorshkov, “Asymmetric particle transport and light-cone dy-

- namics induced by anyonic statistics,” *Phys. Rev. Lett.* **121**, 250404 (2018).
- [70] G. Vidal, “Efficient classical simulation of slightly entangled quantum computations,” *Phys. Rev. Lett.* **91**, 147902 (2003).
- [71] U. Schollwöck, “The density-matrix renormalization group in the age of matrix product states,” *Annals of physics* **326**, 96 (2011).
- [72] J. Li, R. Fan, H. Wang, B. Ye, B. Zeng, H. Zhai, X. Peng, and J. Du, “Measuring out-of-time-order correlators on a nuclear magnetic resonance quantum simulator,” *Phys. Rev. X* **7**, 031011 (2017).
- [73] X. Nie, B.-B. Wei, X. Chen, Z. Zhang, X. Zhao, C. Qiu, Y. Tian, Y. Ji, T. Xin, D. Lu, and J. Li, “Experimental observation of equilibrium and dynamical quantum phase transitions via out-of-time-ordered correlators,” *Phys. Rev. Lett.* **124**, 250601 (2020).
- [74] M. Gärtner, J. G. Bohnet, A. Safavi-Naini, M. L. Wall, J. J. Bollinger, and A. M. Rey, “Measuring out-of-time-order correlations and multiple quantum spectra in a trapped-ion quantum magnet,” *Nat. Phys.* **13**, 781 (2017).
- [75] K. A. Landsman, C. Figgatt, T. Schuster, N. M. Linke, B. Yoshida, N. Y. Yao, and C. Monroe, “Verified quantum information scrambling,” *Nature* **567**, 61 (2019).
- [76] M. K. Joshi, A. Elben, B. Vermersch, T. Brydges, C. Maier, P. Zoller, R. Blatt, and C. F. Roos, “Quantum information scrambling in a trapped-ion quantum simulator with tunable range interactions,” *Phys. Rev. Lett.* **124**, 240505 (2020).
- [77] A. M. Green, A. Elben, C. H. Alderete, L. K. Joshi, N. H. Nguyen, T. V. Zache, Y. Zhu, B. Sundar, and N. M. Linke, “Experimental measurement of out-of-time-ordered correlators at finite temperature,” [arXiv:2112.02068](https://arxiv.org/abs/2112.02068) (2021).
- [78] X. Mi, P. Roushan, C. Quintana, S. Mandrà, J. Marshall, C. Neill, F. Arute, K. Arya, J. Atalaya, R. Babbush, *et al.*, “Information scrambling in quantum circuits,” *Science*, [eabg5029](https://doi.org/10.1126/science.1234567) (2021).
- [79] M. S. Blok, V. V. Ramasesh, T. Schuster, K. O’Brien, J. M. Kreikebaum, D. Dahlen, A. Morvan, B. Yoshida, N. Y. Yao, and I. Siddiqi, “Quantum information scrambling on a superconducting qutrit processor,” *Phys. Rev. X* **11**, 021010 (2021).
- [80] J. Braumüller, A. H. Karamlou, Y. Yanay, B. Kannan, D. Kim, M. Kjaergaard, A. Melville, B. M. Niedzielski, Y. Sung, A. Vepsäläinen, *et al.*, “Probing quantum information propagation with out-of-time-ordered correlators,” [arXiv:2102.11751](https://arxiv.org/abs/2102.11751) (2021).
- [81] Q. Zhu, Z.-H. Sun, M. Gong, F. Chen, Y.-R. Zhang, Y. Wu, Y. Ye, C. Zha, S. Li, S. Guo, *et al.*, “Observation of thermalization and information scrambling in a superconducting quantum processor,” [arXiv:2101.08031](https://arxiv.org/abs/2101.08031) (2021).
- [82] M. Saffman, “Quantum computing with atomic qubits and Rydberg interactions: Progress and challenges,” *J. Phys. B At. Mol. Opt. Phys.* **49**, 202001 (2016).
- [83] A. Browaeys and T. Lahaye, “Many-body physics with individually controlled rydberg atoms,” *Nat. Phys.* **16**, 132 (2020).
- [84] D. Hahn, P. A. McClarty, and D. J. Luitz, “Information dynamics in a model with hilbert space fragmentation,” [arXiv:2104.00692](https://arxiv.org/abs/2104.00692) (2021).
- [85] V. Khemani, M. Hermele, and R. Nandkishore, “Localization from hilbert space shattering: From theory to physical realizations,” *Phys. Rev. B* **101**, 174204 (2020).
- [86] B. Buča, “Local hilbert space fragmentation and out-of-time-ordered crystals,” [arXiv:2108.13411](https://arxiv.org/abs/2108.13411) (2021).
- [87] D. Mondal, S. Sinha, and S. Sinha, “Dynamical route to ergodicity and quantum scarring in kicked coupled top,” *Phys. Rev. E* **104**, 024217 (2021).
- [88] S. Sinha, S. Ray, and S. Sinha, “Fingerprint of chaos and quantum scars in kicked dicke model: an out-of-time-order correlator study,” *J. Phys.: Condens. Matter* **33**, 174005 (2021).
- [89] N. Bao and H. Ooguri, “Distinguishability of black hole microstates,” *Phys. Rev. D* **96**, 066017 (2017).
- [90] W.-z. Guo, F.-L. Lin, and J. Zhang, “Distinguishing black hole microstates using holevo information,” *Phys. Rev. Lett.* **121**, 251603 (2018).
- [91] S. Sachdev and J. Ye, “Gapless spin-fluid ground state in a random quantum heisenberg magnet,” *Phys. Rev. Lett.* **70**, 3339 (1993).
- [92] A. Kitaev, “A simple model of quantum holography,” [Talk at KITP, University of California, Santa Barbara](https://arxiv.org/abs/1505.04311) (2015).
- [93] Y. Gu, X.-L. Qi, and D. Stanford, “Local criticality, diffusion and chaos in generalized sachdev-ye-kitaev models,” *J. High Energy Phys.* **2017**, 1 (2017).
- [94] Y. Gu, A. Kitaev, and P. Zhang, “A two-way approach to out-of-time-order correlators,” [arXiv:2111.12007](https://arxiv.org/abs/2111.12007) (2021).
- [95] H. Bruus and K. Flensberg, *Many-body quantum theory in condensed matter physics: an introduction* (OUP Oxford, 2004).
- [96] K. Sacha and J. Zakrzewski, “Time crystals: a review,” *Rep. Prog. Phys.* **81**, 016401 (2017).
- [97] D. V. Else, C. Monroe, C. Nayak, and N. Y. Yao, “Discrete time crystals,” *Annu. Rev. Condens. Matter Phys.* **11**, 467 (2020).
- [98] B. Huang, Y.-H. Wu, and W. V. Liu, “Clean floquet time crystals: Models and realizations in cold atoms,” *Phys. Rev. Lett.* **120**, 110603 (2018).
- [99] M. Fishman, S. R. White, and E. M. Stoudenmire, “The itensor software library for tensor network calculations,” [arXiv:2007.14822](https://arxiv.org/abs/2007.14822) (2020).
- [100] B. Vermersch, A. Elben, L. M. Sieberer, N. Y. Yao, and P. Zoller, “Probing scrambling using statistical correlations between randomized measurements,” *Phys. Rev. X* **9**, 021061 (2019).
- [101] R. J. Garcia, Y. Zhou, and A. Jaffe, “Quantum scrambling with classical shadows,” *Phys. Rev. Research* **3**, 033155 (2021).

Supplementary Materials for: Quantum Information Scrambling in Quantum Many-body Scarred Systems

ANALYTICAL EXPLANATIONS

In this section, we provide detailed analytical explanations for the OTOC and Holevo information dynamics in quantum many-body scarred systems. First, we need to mention that the analytical computation of OTOCs is a challenging task for general quantum many-body systems, despite a few pronounced solvable examples such as the Sachdev-Ye-Kitaev (SYK) model [91–94]. For the PXP model, it is difficult to directly deal with its OTOC dynamics by the perturbation method since all the terms in the Hamiltonian have the same interaction strength. However, the essential features of the PXP model consist of two parts: the periodic revivals within and the chaotic dynamics out of the scarred subspace, which can be described by a phenomenological model proposed in [31]:

$$H' = H'_0 + R = \frac{\Omega}{2} \sum_i \sigma_i^x + \sum_i R_{i,i+3} P_{i+1,i+2}, \quad (\text{S1})$$

where $P_{i,i+1} = (1 - \vec{\sigma}_i \cdot \vec{\sigma}_{i+1})/4$ is the projector towards the singlet state of spins $i, i+1$, and $R_{i,j} = \sum_{\mu,\nu} J_{ij}^{\mu\nu} \sigma_i^\mu \sigma_j^\nu$ ($J_{ij}^{\mu\nu}$ are random coupling constants, $\mu, \nu = \{x, y, z\}$). The H'_0 and R terms characterize the periodic revivals and thermalization effect in the PXP model respectively. Below we consider a 1D open boundary chain with $L/2$ -spins.

The $L+1$ scarred eigenstates of H' are all the x -direction Dicke states $|s = L/2, S^x = m^x\rangle$, namely the $L+1$ states of the angular momentum $s = L/2$ with x -component $m_x = -s, -s+1, \dots, s-1, s$. Since any Dicke state has an explicit Schmidt decomposition:

$$|s = \frac{L}{2}, S^x = l - \frac{L}{2}\rangle = \sum_{n=0}^N \sqrt{P_n(l)} |s = \frac{N}{2}, S^x = n - \frac{N}{2}\rangle |s = \frac{L-N}{2}, S^x = l - n - \frac{L-N}{2}\rangle, \quad (\text{S2})$$

where $P_n(l) = \binom{N}{n} \binom{L-N}{l-n} / \binom{L}{l}$, and $P_{i,i+1} |s = 1, S^x = -1, 0, 1\rangle_{i,i+1} = 0 \quad \forall i$, we have $P_{i,i+1} |s = L/2, S^x = m^x\rangle = 0 \quad \forall i, m_x$. We hence deduce that

$$H' |s = \frac{L}{2}, S^x = m^x\rangle = H'_0 |s = \frac{L}{2}, S^x = m^x\rangle = m_x \Omega |s = \frac{L}{2}, S^x = m^x\rangle. \quad (\text{S3})$$

These scarred eigenstates form an exact $su(2)$ algebra (while the scars in the PXP model form an approximate one) [31], leading to the periodic revival dynamics governed by the global Rabi oscillation term H'_0 , from initial states within the scarred subspace (for example, the z -direction Dicke states like $|\psi\rangle = |\uparrow\uparrow \dots \uparrow\rangle$). In contrast, initial states out of the scarred subspace can not be projected out by $P_{i,i+1}$, thus are affected by the $R_{i,i+3}$ terms and have chaotic dynamics.

The OTOC operator $F_{ij}(t) = \langle \psi | W_i^\dagger V_j^\dagger(t) W_i V_j(t) | \psi \rangle$ can be viewed as the overlap between two time-dependent quantum states $F_{ij}(t) = \langle \psi_2(t) | \psi_1(t) \rangle$:

$$|\psi_1(t)\rangle = W_i e^{iHt} V_j e^{-iHt} |\psi\rangle \quad |\psi_2(t)\rangle = e^{iHt} V_j e^{-iHt} W_i |\psi\rangle. \quad (\text{S4})$$

First of all, for the ZZ -OTOC case of the PXP model with the initial state $|Z_2\rangle$ (or the H' model above with the initial state $|\psi\rangle = |\uparrow\uparrow \dots \uparrow\rangle$), since $|Z_2\rangle$ ($|\psi\rangle$) is the eigenstate of the $\sigma_{i(j)}^z$ operator, the periodic revival dynamics of the quantum state directly give us the periodic and synchronized oscillations of the ZZ -OTOC $F_{ij}(t)$. Note that the oscillation period of the ZZ -OTOC is supposed to be $T/2 = \pi/\Omega$, which is indeed true for the H' model with perfect quantum many-body scars. Because after $T/2$ evolution, $|Z_2\rangle$ evolves to $|Z'_2\rangle = (\prod_{i=1}^L \sigma_i^x) |Z_2\rangle$ ($|\uparrow\uparrow \dots \uparrow\rangle$ evolves to $|\downarrow\downarrow \dots \downarrow\rangle$), which is again the eigenstate of the $\sigma_{i(j)}^z$. However, the periodic revival dynamics and emergent $su(2)$ algebra of the PXP model are not perfect [31], resulting in smaller peak values of $F_{ij}(t = (2n+1)T/2)$ than those of $F_{ij}(t = nT)$ ($n = 0, 1, 2, \dots$). Eventually we observe an overall oscillation period $T = 2\pi/\Omega$ in numerical simulations. Specially for the PXP model, since we consider the dynamics within the constrained Hilbert space (where computational bases with two nearby up spins $|\dots \uparrow\uparrow \dots\rangle$ are removed), only the ZZ -OTOC dynamics for generic initial states $|\psi\rangle$ are legal, namely within the constrained Hilbert space. The XZ -OTOCs for the $|Z_2\rangle$ initial state with $W_i = \sigma_i^x$ acting on an up spin $|\uparrow\rangle_i$ are also legal and have well-defined physical meanings in the overlap interpretation Eq. (S4). Fortunately, the problem of constrained Hilbert space does not appear in the H' model above. Besides, the Holevo information dynamics for general initial states are also not well defined, since it will be difficult to locally encode 1 bit information on general initial states, for example the scarred eigenstates.

Now we consider the non-trivial XZ -OTOC dynamics of H' with the initial state $|\psi\rangle = |\uparrow\uparrow\cdots\uparrow\rangle$. For $W_1 = \sigma_1^x$, $V_r = \sigma_r^z$, $t = nT/2$ ($n = 0, 1, 2, \dots$), according to Eq. (S4),

$$|\psi_1(t)\rangle = \sigma_1^x e^{iH't} \sigma_r^z e^{-iH't} |\psi\rangle = (-1)^n \sigma_1^x |\psi\rangle \quad |\psi_2(t)\rangle = e^{iH't} \sigma_r^z e^{-iH't} \sigma_1^x |\psi\rangle, \quad (\text{S5})$$

$$F(r, t) = \langle \psi_2(t) | \psi_1(t) \rangle = (-1)^n \langle \phi(t) | \sigma_r^z | \phi(t) \rangle. \quad (\text{S6})$$

Here by utilizing the property of state recurrence, we successfully convert the four-body OTOC into an observable average on a time-dependent quantum state $|\phi(t)\rangle = e^{-iH't} \sigma_1^x |\psi\rangle$. The physical picture for the formation of linear light cone structure in OTOC and Holevo information dynamics can be summarized as follows: without the action of σ_1^x , the state $|\phi(t)\rangle$ will undergo perfect periodic oscillations, thus $F(r, t = nT/2) \equiv 1$; However, now σ_1^x penetrates the scarred subspace on the first site. The ‘‘heat flow’’ (like a quasi-particle created by the local quench [20]) leaks and propagates ballistically through the entire system, leading to the decay of OTOC $F(r, t = nT/2) < 1$ after the wavefront of heat flow arrives. Note that in the setup of Holevo information dynamics, we also have a Hamiltonian evolution term $e^{-iH't} \sigma_{[L/2]}^x |Z_2\rangle$, which has the same structure of $|\phi(t)\rangle$. We hence deduce that the dynamics of Holevo information and OTOCs are closely related and follow the same physical picture. Indeed the numerical results of the two criteria support each other and exhibit similar information scrambling behaviors.

In order to further explore the role of the R thermalization term, we adopt the interaction picture of $H'_0 = (\Omega/2) \sum_i \sigma_i^x$ to remove the Rabi oscillation effect. We denote the quantum states and operators in the interaction picture with hats:

$$|\hat{\phi}(t)\rangle = e^{iH'_0 t} |\phi(t)\rangle \quad \hat{R}(t) = e^{iH'_0 t} R e^{-iH'_0 t}. \quad (\text{S7})$$

The quantum state evolution in the H'_0 interaction picture is

$$i\partial_t |\hat{\phi}(t)\rangle = \hat{R}(t) |\hat{\phi}(t)\rangle, \quad (\text{S8})$$

$$|\hat{\phi}(t)\rangle = \hat{U}(t) |\hat{\phi}(0)\rangle = \hat{U}(t) \sigma_1^x |\psi\rangle \quad \hat{U}(t) = T_t \left(\exp(-i \int_0^t dt' \hat{R}(t')) \right), \quad (\text{S9})$$

where we have introduced the time ordering operator T_t . According to Eq. (S6), at the special time points $t = nT/2$, the OTOCs in the interaction picture have the expression

$$F(r, t) = (-1)^n \langle \hat{\phi}(t) | e^{iH'_0 t} \sigma_r^z e^{-iH'_0 t} | \hat{\phi}(t) \rangle = (-1)^n \langle \hat{\phi}(t) | e^{i\Omega\sigma_r^x t/2} \sigma_r^z e^{-i\Omega\sigma_r^x t/2} | \hat{\phi}(t) \rangle = \langle \hat{\phi}(t) | \sigma_r^z | \hat{\phi}(t) \rangle. \quad (\text{S10})$$

Below we consider the so-called early growth region of the OTOC, namely the time interval from $t = 0$ to the time t just before the wavefront of heat flow arrives at the site r . Then we can split the evolution time t into r pieces with $\Delta t = t/r$, $J\Delta t \ll 1$ (J is the average energy scale of all the $J_{ij}^{\mu\nu}$), to treat the dynamics perturbatively:

$$\begin{aligned} \hat{U}(t) &= T_t \left(\exp(-i \int_0^t dt' \hat{R}(t')) \right) \\ &= \prod_{n=0}^{r-1} \exp(-i \int_{n\Delta t}^{(n+1)\Delta t} dt' \hat{R}(t')) \\ &\approx \prod_{n=0}^{r-1} (1 - i\hat{R}(n\Delta t)\Delta t), \end{aligned} \quad (\text{S11})$$

where $\hat{R}(n\Delta t) = \sum_i \hat{R}^i(n\Delta t) = \sum_i \left(e^{iH'_0 n\Delta t} R_{i,i+3} P_{i+1,i+2} e^{-iH'_0 n\Delta t} \right)$. According to Eq. (S9) and (S10), besides the leading 1 term in Eq. (S11), the OTOC $F(r, t = nT/2)$ will be dominantly influenced by the following operator product series:

$$(-i)^r (\Delta t)^r \hat{R}^r((r-1)\Delta t) \cdots \hat{R}^2(\Delta t) \hat{R}^1(0) \sigma_1^x |\psi\rangle. \quad (\text{S12})$$

The operator product series Eq. (S12) vividly characterizes propagation of the thermalization effect from the site 1 to site r . Since H'_0 only contains single-body operators, other $\hat{R}^i(n\Delta t)$ operator product series acting on $\sigma_1^x |\psi\rangle$ will either be zero due to the projectors $P_{i,i+1}$, or unable to reach the site r and affect the perfect revival dynamics. Inserting Eq. (S12) into Eq. (S10), we obtain that the leading correction term of the OTOC $F(r, t = nT/2)$ can be bounded by

$$||[\sigma_r^z, \hat{R}^r((r-1)\Delta t) \cdots \hat{R}^2(\Delta t) \hat{R}^1(0)]_{\pm}|| (\Delta t)^r \leq (aJ\Delta t)^r, \quad (\text{S13})$$

where a is some model-dependent $O(1)$ constant, $[\cdot]_{\pm}$ denotes commutator(-) and anti-commutator(+), and $\|\cdot\|$ denotes the operator norm. The bound in Eq. (S13) does not depend on T or Ω (which stands for the resolution in time), so we are able to generalize the special time points $t = nT/2$ to arbitrary t before the wavefront arrives. Finally we have the following OTOC behaviors in the early growth region:

$$F(r, t) \sim 1 - \left(\frac{aJt}{r}\right)^r. \quad (\text{S14})$$

Eq. (S14) readily depicts a linear light cone structure $t \propto r/J$ in the early growth region. While we specifically compute the XZ -OTOC of the phenomenological model Eq. (S1), the physical pictures of local thermalization and ballistic propagation hold for other quantum many-body scarred systems, other OTOCs and Holevo information dynamics, and can be applied to explain the linear light cone structure observed in the numerical simulation results.

Despite the fact that the OTOC dynamics have linear light cone structure both in the ETH and many-body scarred systems, the thermalization processes are pretty different: in the ETH systems, once we start the Hamiltonian evolution, thermalization happens everywhere *globally* on the quantum states; on the contrary for many-body scarred systems, according to the calculations above, the periodic revivals are destroyed *locally* at some sites and the deterioration effect then propagates through the entire system. The global versus local thermalization processes are reminiscent of the spin correlation dynamics in global [19] versus local [20] quench dynamics, and can also explain the larger butterfly velocity for the $|\mathbf{0}\rangle$ initial state than that of the $|Z_2\rangle$ initial state in OTOC and Holevo information dynamics.

Another remark is that the perturbation calculations above are similar to the derivations of Kubo formula in the linear response theory, and the correction term Eq. (S12) corresponds to the r -th order response to the perturbation $\hat{R}(t)$ [95].

The perturbation-type calculations break down for the OTOC and Holevo information dynamics deep inside the light cone. As is mentioned in the main text, the persistent and synchronized oscillations inside the light cone still appear even if the initial states are replaced with scarred eigenstates or superposition states of $|Z_2\rangle$ and $|Z'_2\rangle = (\prod_{i=1}^L \sigma_i^x)|Z_2\rangle$ (see Fig. S2 and S4), which confirms that periodic revivals of OTOCs are general phenomena for initial states within the scarred subspace, not some fine-tuned results. We attribute the unusual revival dynamics inside the light cone to the local rather than global thermalization argued above and robustness of scarred eigenstates against local perturbations: The quantum many-body scars have been shown to present certain robustness against perturbations and disorders [50–54]. Under some local perturbations like the $\sigma_{i(j)}^{x(z)}$ operators ($e^{-iH't} \sigma_1^x |\psi\rangle$), thermalization happens locally and propagates outwards. After the wavefront of thermalization effect passes, the periodic oscillations of local observables are preserved to some extent due to the robustness of scar eigenstates, leading to the revival pattern observed in the OTOC and Holevo information dynamics.

In this sense, the periodic revival behaviors of OTOCs in quantum many-body scarred systems are pretty similar to the dynamics in time crystals [86, 96–98]: the ZZ -OTOC dynamics for the $|Z_2\rangle$ initial state is an analogue to the time crystals without perturbations; while the XZ -OTOCs for $|Z_2\rangle$ and ZZ -OTOCs for general initial states within the scarred subspace correspond to the perturbed time crystals, which will exhibit certain robustness and maintain the synchronized oscillations. This topic might need deeper understanding and more powerful techniques to deal with, so that is expected to inspire in-depth analytical studies in future.

Another possible perspective is about relations with the classical OTOC and chaos theory [32–34, 87, 88]. According to the quantum-classical correspondence principle, we may replace the quantum commutators in the OTOC with classical Poisson brackets. By utilizing the semi-classical Lagrangian of quantum many-body scarred systems, like the one proposed in [32] with the time-dependent variational principle (TDVP), we are able to compute the Poisson brackets ($\{\cdot\}_{P.B.}$) of some observables like $\{\cos \theta_i(t), \cos \theta_j(0)\}_{P.B.} \sim \sin \theta_i(t) \frac{\partial \theta_i(t)}{\partial \theta_i(0)}$ (θ is the polar angle on the spin-1/2 Bloch sphere). The oscillating dynamics of $\sin^2 \theta_i(t)$ terms from some special initial states like $|Z_2\rangle$ will roughly lead to the periodic revivals of classical OTOCs.

NUMERICAL METHODS AND MORE RESULTS

In this section, we illustrate the numerical methods used in the main text and provide more numerical results of the OTOC and Holevo information dynamics in quantum many-body scarred systems. We numerically simulate the ZZ - and XZ -OTOC dynamics of the PXP model using the time-splitting matrix product operator (MPO) method [58, 59] up to system size $L = 41$, with the maximum bond dimension 300 and a Trotter step $dt = 0.05$. Fig. S1 displays a pictorial illustration of the algorithm. Specifically, we rewrite the OTOC $F_{ij}(t) = \langle \psi | W_i^\dagger V_j^\dagger(t) W_i V_j(t) | \psi \rangle$ as

$$F_{ij}(t) = \langle \psi(t/2) | W_i^\dagger(-t/2) V_j^\dagger(t/2) W_i(-t/2) V_j(t/2) | \psi(t/2) \rangle, \quad (\text{S15})$$

where $|\psi(t/2)\rangle = e^{-iHt/2} |\psi\rangle$. Usually in order to maintain the simulation accuracy, we need to increase the bond dimension when extending the evolution time t , because of the increase of entanglement entropy. Here by equally splitting the Hamiltonian

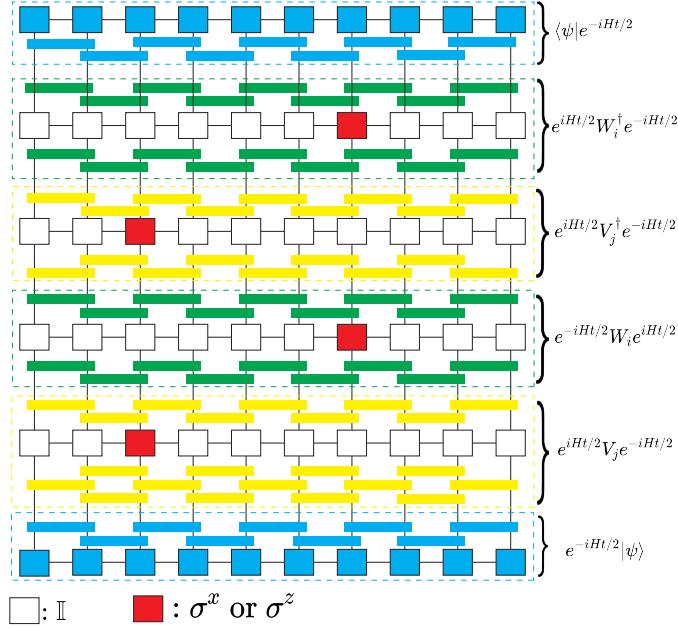


FIG. S1. The time-splitting MPO algorithm for OTOC calculations. The blue squares denote MPS tensors and the white (red) squares denote MPO tensors. All the rectangles stand for the Trotterized Hamiltonian evolution blocks. The total evolution time t has been equally split to each part of $F_{ij}(t) = \langle \psi(t/2) | W_i^\dagger(-t/2) V_j^\dagger(t/2) W_i(-t/2) V_j(t/2) | \psi(t/2) \rangle$ to reduce the required bond dimension. The overall contraction of the tensor network above will give the OTOC $F_{ij}(t)$.

evolution to each part of $F_{ij}(t)$, we are able to reduce the support of the scrambled operators $V_j(t)$. For a fixed evolution time, this algorithm leads to notable reduction of the required bond dimension compared with previous MPO algorithms [58, 71].

We use the time-evolving block decimation (TEBD) algorithm [70, 71] based on the matrix product state (MPS) ansatz to simulate the Holevo information dynamics for the PXP model up to system size $L = 41$, with the maximum bond dimension 100 and a Trotter step $dt = 0.05$. The relatively low entanglement entropy of scarred eigenstates [Fig. S3(b) and S5(b)] makes the simulations from the initial state $|Z_2\rangle$ much more efficient, yet this advantage no more exists for the $|0\rangle$ case. All the MPO and MPS based numerical simulations are carried out with the ITensor library [99].

Numerical calculations for small system size ($L \sim 20$) are performed with the exact diagonalization (ED) method in the constrained Hilbert space of the PXP model, for instance, Fig. 2(f) and Fig. 3 of the main text.

In the main text, we have shown that the OTOC dynamics exhibit exotic periodic revivals inside the light cone for the initial state $|Z_2\rangle$. In Fig. S2 and Fig. S4, we present the ZZ -OTOC dynamics of the PXP model for more general initial states in the open boundary condition (with boundary terms $\sigma_1^x P_2$ and $P_{L-1} \sigma_L^x$) and periodic boundary condition, respectively. First the ZZ -OTOC dynamics for superposition states of $|Z_2\rangle$ and $|Z'_2\rangle = \prod_i \sigma_i^x |Z_2\rangle$ are displayed in Fig. S2(a), (b). Second, in Fig. S2(c)-(i), we take the energy eigenstates of the PXP Hamiltonian as initial states for the ZZ -OTOC calculations. The eigenstates are marked with the corresponding labels in Fig. S3. We observe that despite lower oscillation contrast compared to the $|Z_2\rangle$ case, the pattern of persistent and synchronized oscillations for ZZ -OTOCs still exists for the superposition states of $|Z_2\rangle$ and $|Z'_2\rangle$ (a)-(b), scarred energy eigenstates (c)-(g), and also general superposition states of scarred eigenstates. However, the oscillation pattern is absent for typical thermal eigenstates (h)-(i). The numerical results indicate that the periodic revivals of OTOCs inside the light cone are not some fine-tuned results for the initial state $|Z_2\rangle$, but a general phenomenon for a certain class of states within the non-thermal scarred subspace. The information scrambling dynamics for quantum many-body scarred systems are intrinsically different from the ETH or MBL cases. One additional remark is that we have calculated the ZZ -OTOC dynamics for all the scarred eigenstates marked in Fig. S3 and found that the periodic oscillation pattern always exists while the oscillation contrast fades away for a few scarred eigenstates near the ground state, which is probably due to the finite size effect.

In order to distinguish the scarred eigenstates and typical thermal eigenstates, we show the overlap between the $|Z_2\rangle$ state and each energy eigenstate $|E_n\rangle$ of the PXP Hamiltonian with the open boundary condition in Fig. S3(a), and the half-chain entanglement entropy S of energy eigenstates in Fig. S3(b) [11, 12]. All the scarred eigenstates and two thermal eigenstates in the bulk are marked by labels consistent with those in Fig. S2. The half-chain entanglement entropy of two scarred eigenstates near $E = 0$ is relatively larger compared with other scarred eigenstates, which is probably due to the open boundary condition. In order to rule out the possible effects of boundary conditions, we display the corresponding results of the PXP model in the

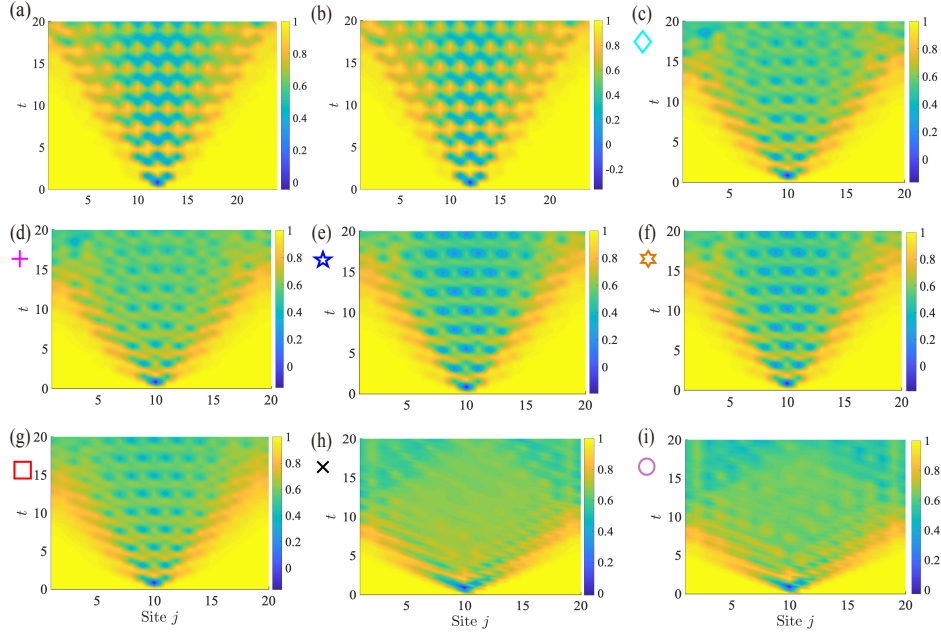


FIG. S2. Numerical simulations of ZZ -OTOC dynamics for the $L = 20$ PXP model in the open boundary condition, with initial states being (a) $\frac{1}{\sqrt{2}}(|Z_2\rangle + |Z'_2\rangle)$, $|Z_2\rangle = \prod_i \sigma_i^x |Z_2\rangle$; (b) $\sqrt{\frac{2}{3}}|Z_2\rangle + \sqrt{\frac{1}{3}}|Z'_2\rangle$; (c)-(f) scarred and thermal energy eigenstates, marked by the same labels in Fig. S3.

periodic boundary condition in Fig. S4 and Fig. S5. Compared with Fig. S2 and Fig. S3, these results do not show distinct differences despite different boundary conditions.

We present more numerical simulations of ZZ -OTOC and Holevo information dynamics of the experimental Rydberg-atom Hamiltonian (Eq. (5) and related \mathcal{H}_\pm in the main text) in Fig. S6 to demonstrate their measurable signatures. In plots (a), (d), the experimental parameters are the same as those used in [9], where $\Omega = 2$, $U_1 = 24$, $U_2 = 0.38$ and $\Delta = 0$. We observe that the periodic oscillations display a much lower contrast than that of the PXP model, which is induced by the invalidity of the condition $U_1 \gg \Omega \gg U_2$. Constrained by the geometry of 1D equally-spaced atoms, $U_1/U_2 \sim 64$ is fixed, such that Ω around $\sqrt{U_1 U_2}$ can best fulfill the condition above. With this motivation, we show the results in plots (b), (e), with parameters $\Omega = 1.5$, $U_1 = 12$, $U_2 = 0.19$ and $\Delta = 0.19$. We observe that the oscillation pattern could be identified more clearly. As is mentioned in the main text, we have further added a non-zero detuning Δ , in order to offset the influence induced by U_2 . Through the simple grid search optimization of the parameters Ω and Δ , in plots (c), (f), among several instances with relatively high oscillation contrast, we display the one with parameters $\Omega = 2$, $U_1 = 12$, $U_2 = 0.19$ and $\Delta = 0.38$, which is the 2D view of Fig. 3 in the main text. The linear light cone contour and periodic oscillations inside the light cone can be readily observed.

In the main text, we have numerically calculated the XZ -OTOC dynamics of the PXP model. However, XZ -OTOCs can not be directly reduced to the observable average form like Eq. (6) of the main text, thus do not have a similar measurement scheme like the ZZ -OTOCs. Several other methods such as the ones based on randomized measurements [100] or classical shadow estimations [101] might be modified and adopted instead.

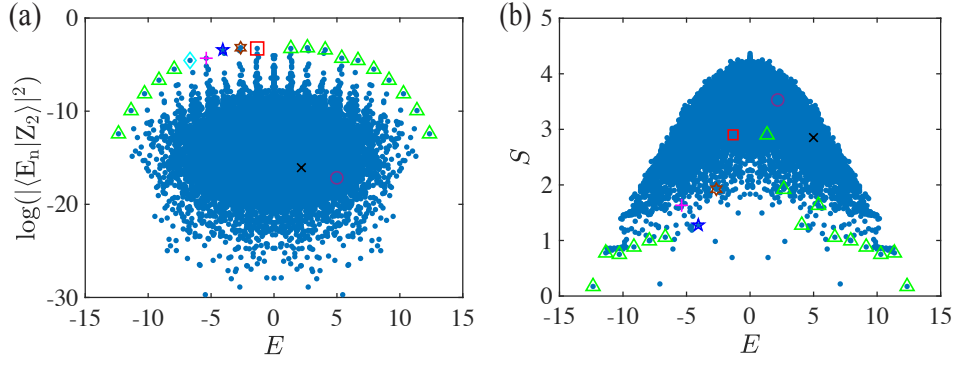


FIG. S3. (a) Overlap between the $|Z_2\rangle$ state and each energy eigenstate $|E_n\rangle$ of a $L = 20$ PXP model with the open boundary condition. (b) The half-chain entanglement entropy S for each energy eigenstate. The scarred eigenstates form a special band in the top of plot (a). The scars together with two thermal eigenstates in the bulk are marked by labels consistent with those in Fig. S2.

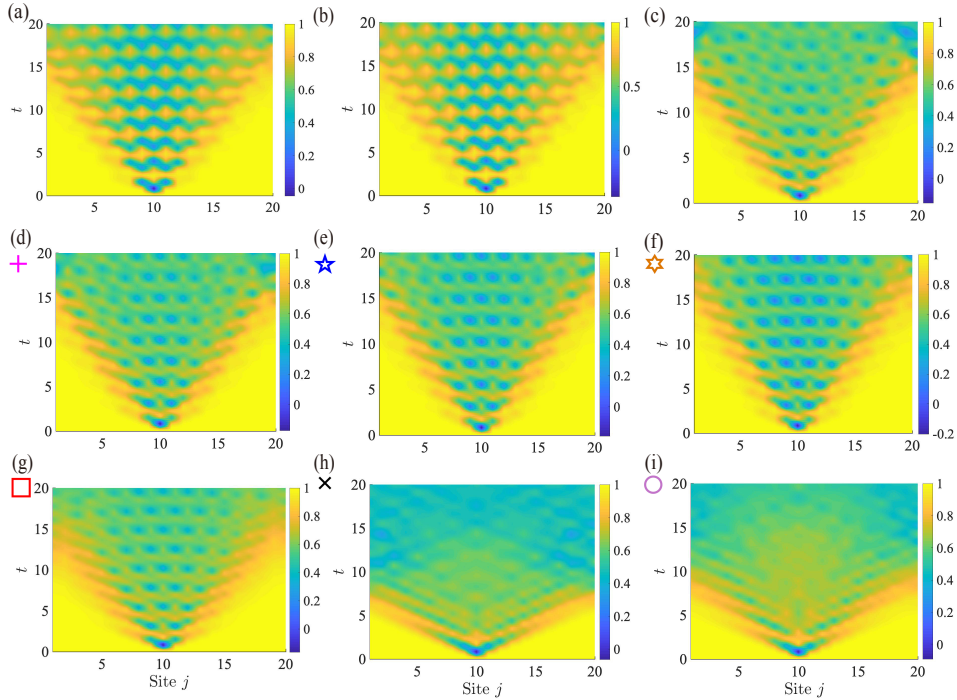


FIG. S4. Numerical simulations of ZZ -OTOC dynamics for the $L = 20$ PXP model in the periodic boundary condition, with initial states being (a) $\frac{1}{\sqrt{2}}(|Z_2\rangle + |Z'_2\rangle)$, $|Z'_2\rangle = \prod_i \sigma_i^x |Z_2\rangle$; (b) $\sqrt{\frac{2}{3}}|Z_2\rangle + \sqrt{\frac{1}{3}}|Z'_2\rangle$; (c)-(f) scarred and thermal energy eigenstates, marked by the same labels in Fig. S5.

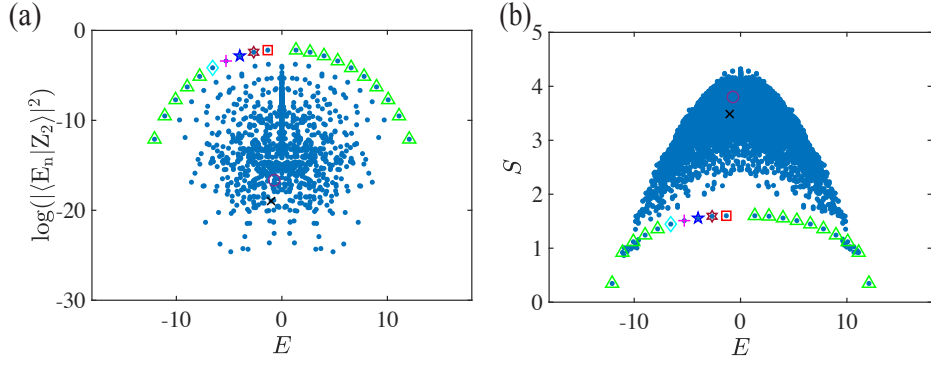


FIG. S5. (a) Overlap between the $|Z_2\rangle$ state and each energy eigenstate $|E_n\rangle$ of a $L = 20$ PXP model with the periodic boundary condition. (b) The half-chain entanglement entropy S for each energy eigenstate. The scarred eigenstates form a special band in the top of plot (a). The scars together with two thermal eigenstates in the bulk are marked by labels consistent with those in Fig. S4.

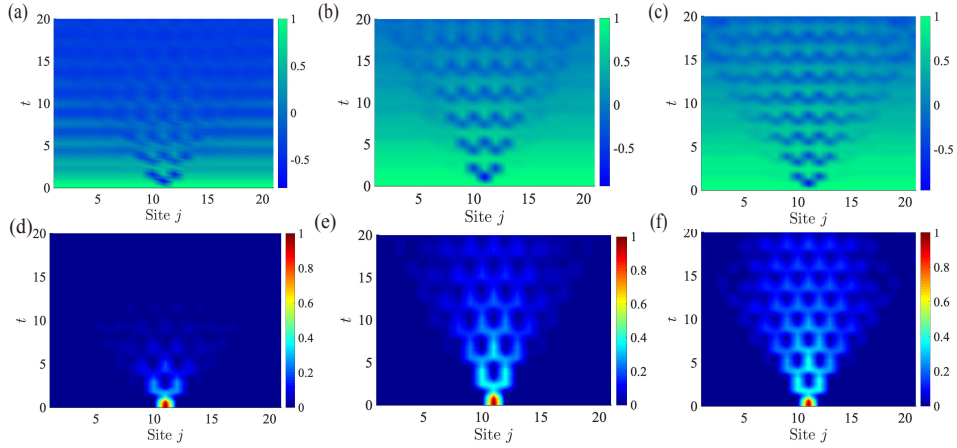


FIG. S6. Numerical simulations of the ZZ -OTOC dynamics (a)-(c) and Holevo information dynamics (d)-(f) for the experimental Rydberg-atom Hamiltonian, with the initial state $|Z_2\rangle$ and experimental parameters: (a), (d) $L = 21$, $\Omega = 2$, $U_1 = 24$, $U_2 = 0.38$ and $\Delta = 0$; (b), (e) $L = 21$, $\Omega = 1.5$, $U_1 = 12$, $U_2 = 0.19$ and $\Delta = 0.19$; (c), (f) $L = 21$, $\Omega = 2$, $U_1 = 12$, $U_2 = 0.19$ and $\Delta = 0.38$.